IMA Journal of Applied Mathematics (2006) 1−16
doi:10.1093/imamat/hxh111

A Lobatto interpolation grid in the tetrahedron

H. LUO AND C. POZRIKIDIS
Department of Mechanical and Aerospace Engineering, University of California, San Diego, La Jolla, CA 92093-0411, USA

[Received on 29 April 2005; revised on 15 November 2005; accepted on 21 November 2005]

A sequence of increasingly refined interpolation grids inside the tetrahedron is proposed with the goal of achieving uniform convergence and ensuring high interpolation accuracy. The number of interpolation nodes, N, corresponds to the number of terms in the complete mth-order polynomial expansion with respect to the three tetrahedral barycentric coordinates. The proposed grid is constructed by deploying Lobatto interpolation nodes over the faces of the tetrahedron, and then computing interior nodes using a simple formula that involves the zeros of the Lobatto polynomials. Numerical computations show that the Lebesgue constant and interpolation accuracy of the proposed grid compare favourably with those of alternative grids constructed by solving optimization problems. The condition number of the mass matrix is significantly lower than that of the uniform grid and comparable to that of optimal grids proposed by previous authors.

Keywords: interpolation; tetrahedron; Lobatto polynomials; Fekete points; finite elements.

1. Introduction

We consider the polynomial interpolation of a function, f, inside a standard orthogonal tetrahedron in the $\xi\eta\zeta$ space. The four vertices of the standard tetrahedron are located at the origin and along the three Cartesian axes at positions $(1, 0, 0)$, $(0, 1, 0)$ and $(0, 0, 1)$. A complete mth-degree interpolating polynomial, p_m, defined inside the tetrahedron, can be expressed in a series of basis functions that constitute a complete base of the mth-degree polynomial space, ϕ_i, $i = 1, 2, \ldots, N$, as

$$f(\xi, \eta, \zeta) \approx p_m(\xi, \eta, \zeta) = \sum_{i=1}^{N} b_i \phi_i(\xi, \eta, \zeta), \tag{1.1}$$

where b_i are unknown coefficients. The number of terms in the expansion, N, is related to the polynomial order, m, by

$$N = \binom{m+3}{3} = \frac{1}{6}(m+1)(m+2)(m+3). \tag{1.2}$$

One possible choice of basis functions is the family of monomial products, $\phi_i = \xi^p \eta^q \zeta^r$, where p, q and r are non-negative integers. Better choices are provided by the orthogonal polynomials discussed in Section 2, and by the partially orthogonal hierarchical polynomials used in the finite-element modal expansion discussed by Sherwin & Karniadakis (1995, 1996) and Karniadakis & Sherwin (2004).

To compute the expansion coefficients, b_i, we introduce N interpolation nodes, (ξ_j, η_j, ζ_j), inside, over faces and at the vertices of the tetrahedron, enforce the interpolation conditions

$$f(\xi_j, \eta_j, \zeta_j) = p_m(\xi_j, \eta_j, \zeta_j) = \sum_{i=1}^{N} b_i \phi_i(\xi_j, \eta_j, \zeta_j), \tag{1.3}$$

for $j = 1, 2, \ldots, N$ and solve the resulting linear system of equations

$$\mathbf{V}^{\mathrm{T}} \cdot \mathbf{b} = \mathbf{f}, \tag{1.4}$$

where $\mathbf{V}$ is the generalized Vandermonde matrix (VDM),

$$V_{ij} \equiv \phi_i(\xi_j, \eta_j, \zeta_j). \tag{1.5}$$

Alternatively, we may construct the interpolating polynomial explicitly in terms of the data using the Lagrange interpolating polynomials, as

$$p_m(\xi, \eta, \zeta) = \sum_{i=1}^{N} f(\xi_i, \eta_i, \zeta_i)\psi_i(\xi, \eta, \zeta). \tag{1.6}$$

The ith-node cardinal interpolation function, $\psi_i(\xi, \eta, \zeta)$, takes the value of unity at the ith node and the value of zero at the remaining nodes, i.e.

$$\psi_i(\xi_j, \eta_j, \zeta_j) = \delta_{ij}, \tag{1.7}$$

where δ_{ij} is Kronecker's delta. The computation of these cardinals will be discussed in later sections.

In finite-element applications, in order to ensure C^0 continuity of the finite-element expansion over the entire solution domain consisting of the union of adjacent tetrahedra, we assign one shared node at each one of the four vertices, distribute $m + 1$ vertex-inclusive shared nodes along each of the six edges and deploy $\frac{1}{2}(m + 1)(m + 2)$ vertex- and edge-inclusive shared nodes in each face. The edge nodes define an mth-degree polynomial with respect to arc length along each edge, and the face nodes define an mth-degree polynomial in two barycentric coordinates in each face. The vertex, edge and face nodes comprise a set of

$$N_{\mathrm{S}} = 2(m^2 + 1) \tag{1.8}$$

surface nodes. When $m \geqslant 4$, these are complemented by

$$N_{\mathrm{I}} = N - N_{\mathrm{S}} = \frac{1}{6}(m - 3)(m - 2)(m - 1) \tag{1.9}$$

interior nodes representing additional degrees of freedom. It is worth noting that the number of interior nodes is equal to the number of terms in the complete $(m - 4)$th-degree polynomial expansion. Table 1 lists N and N_{I} for polynomial order m up to nine.

In the case of a uniform interpolation grid, the nodes are deployed at the positions (ξ_i, η_j, ζ_k), where $\xi_i = (i - 1)/m$, $\eta_j = (j - 1)/m$ and $\zeta_k = (k - 1)/m$. For each value of the index i in the

TABLE 1 *Total number of interpolation nodes, N, and number of interior nodes, N_{I}, in the complete mth-degree polynomial expansion inside a tetrahedron*

m	1	2	3	4	5	6	7	8	9
N	4	10	20	35	56	84	120	165	220
N_{I}	0	0	0	1	4	10	20	35	56

range $i = 1, 2, \ldots, m+1$, the index j takes values in the range $j = 1, 2, \ldots, m+2-i$; and for each doublet (i, j), the index k takes values in the range $k = 1, 2, \ldots, m+3-i-j$. The corresponding Lagrange interpolating polynomials can be constructed explicitly in terms of 1D Lagrange polynomials using a simple formula (e.g. Pozrikidis, 2005). Unfortunately, as the polynomial order is raised, the interpolation error is not necessarily reduced uniformly inside the tetrahedron due to the Runge effect manifested by oscillations in the cardinal interpolation functions.

To prevent the oscillations, we may require that the nodes are distributed such that the magnitude of the ith cardinal interpolation function reaches the maximum value of unity at the ith node, and varies between zero and unity throughout the tetrahedron. In this way, the sum of the absolute value of the interpolation functions is bounded by N at each point inside the tetrahedron. This requirement is satisfied by the Fekete points, which are computed by maximizing the magnitude of the determinant of the VDM defined in (1.5) within the confine of the tetrahedron. Note that, even though the VDM itself depends on the choice of basis functions, ϕ_i, since changing the polynomial base only multiplies the determinant by a constant factor, the maximum and thus the Fekete set is independent of the adopted base and uniquely defined. Fekete sets are available for the 1D interval (scaled zeros of the Lobatto polynomials), for the triangle, for the rectangle and for the hexahedron (tensor product of the 1D Fekete sets), but not for the tetrahedron, as reviewed by Pozrikidis (2005). However, two alternative optimal sets of interpolation nodes are available for the tetrahedron.

Chen & Babuška (1996) computed node distributions inside the tetrahedron by maximizing the magnitude of the determinant of the VDM, as well as by minimizing the L_2 norm

$$\left(\iiint_T \sum_{i=1}^{N} |\psi_i(\xi, \eta, \zeta)|^2 \mathrm{d}\xi \, \mathrm{d}\eta \, \mathrm{d}\zeta \right)^{1/2}, \tag{1.10}$$

subject to two stipulations: the nodes in each face are distributed as in the case of 2D interpolation over the triangle, and the interior point distributions observe the geometrical symmetries of the tetrahedron. Note that the first stipulation disqualifies the first distribution from being called a true Fekete set. Hesthaven & Teng (2000) performed a similar computation by minimizing an electrostatic potential and discovered a different set of optimal nodes for the tetrahedron.

Blyth & Pozrikidis (2005) recently proposed a simple interpolation grid over the triangle, heretoforth referred to as the Lobatto triangle grid (LTR). To generate this grid, a 1D 'master grid' is first introduced comprising a set of $m+1$ points,

$$v_i = \frac{1}{2}(1 + t_i), \tag{1.11}$$

for $i = 2, 3, \ldots, m$, where t_i are the zeros of the $(m-1)$th-degree Lobatto polynomial, $\mathrm{Lo}_{m-1} = L'_m$, a prime denotes a derivative, and L_m is a Legendre polynomial. The end-points are located at $v_1 = 0$ and $v_{m+1} = 1$. Thus, the nodes of the master grid are the zeros of the completed $(m+1)$th-degree Lobatto polynomial,

$$\mathrm{Lo}^c_{m+1}(t) \equiv (t^2 - 1)\mathrm{Lo}_{m-1}(t). \tag{1.12}$$

The nodal coordinates of the LTR over the standard orthogonal triangle in the $\xi\eta$ plane are generated by the formula

$$\xi = \frac{1}{3}(1 + 2v_i - v_j - v_k), \quad \eta = \frac{1}{3}(1 - v_i + 2v_j - v_k), \tag{1.13}$$

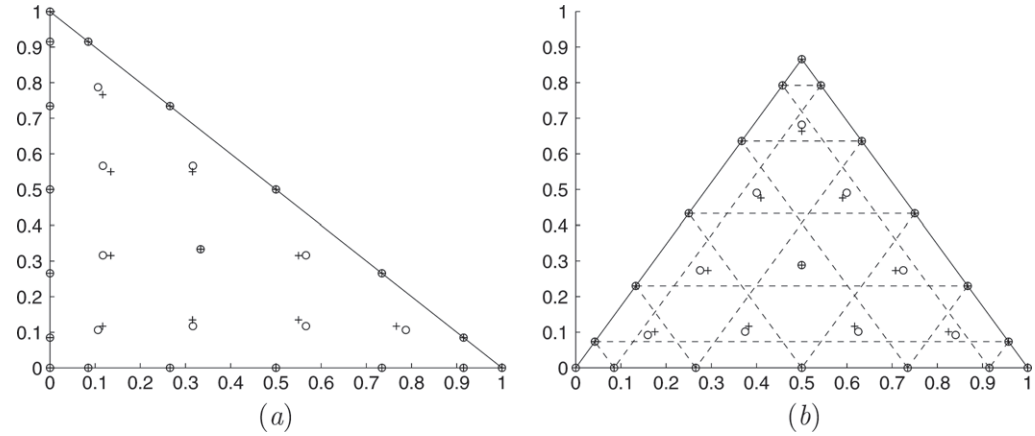

FIG. 1. The Lobatto triangle nodes (+) and associated Fekete nodes (o) over the (a) orthogonal and (b) equilateral triangle for $m = 6$.

for $i = 1, 2, \ldots, m+1$ and $j = 1, 2, \ldots, m+2-i$, where $k = m+3-i-j$. Figure 1 shows the node distribution for $m = 6$ over the standard orthogonal triangle and corresponding equilateral triangle. The corresponding Fekete sets are also shown in this figure after Taylor *et al.* (2000). Geometrically, the LTR nodes are located at the centroids of internal triangles formed by three families of parallel barycentric coordinates, as shown in Fig. 1(b). Note that the LTR nodes are displaced slightly inward with respect to the Fekete nodes. Blyth & Pozrikidis (2005) found that the Lebesgue constant of the LTR compares favourably with that of the optimal Fekete grid.

In this paper, a similar simple construction is proposed for the tetrahedron, coined the Lobatto tetrahedral grid (LTT). First, an optimized interior set is proposed subject to the Lobatto triangle distribution in each face, by maximizing the magnitude of the determinant of the generalized VDM. Second, a simple formula for generating the interior nodes is devised as an extension of the LTR formula for the triangle. The simple formula will be shown to produce results that compare favourably with those obtained using more involved distributions constructed by optimization, and is thus highly recommended in spectral-element implementations.

2. Orthogonal tetrahedral polynomials

Our working polynomial expansion base comprises of the orthogonal tetrahedral polynomials employed by Sherwin & Karniadakis (1995) and further discussed by Karniadakis & Sherwin (2004). To introduce these polynomials, we map the standard tetrahedron in the $\xi\eta\zeta$ space to the standard cube, $-1 \leqslant (\xi', \eta', \zeta') \leqslant 1$, using the transformation

$$\xi = \frac{1+\xi'}{2}\frac{1-\eta'}{2}\frac{1-\zeta'}{2},$$
$$\eta = \frac{1+\eta'}{2}\frac{1-\zeta'}{2},$$
$$\zeta = \frac{1+\zeta'}{2}, \tag{2.1}$$

as illustrated in Fig. 2. The orthogonal tetrahedral polynomials are given by

$$\mathcal{P}_{klp} = L_k(\xi') J_l^{(2k+1,0)}(\eta') J_p^{(2k+2l+2,0)}(\zeta') \left(\frac{1-\eta'}{2}\right)^k \left(\frac{1-\zeta'}{2}\right)^{k+l}, \tag{2.2}$$

where L_k are Legendre polynomials, and $J_k^{(\alpha,\beta)}$ are Jacobi polynomials. Substituting the inverse mapping of (2.1) and cancelling the denominators, we find that $\mathcal{P}_{klp}$ is a kth-degree polynomial in ξ, a $(k+l)$th-degree polynomial in η and a $(k+l+p)$th-degree polynomial in ζ.

The first few tetrahedral orthogonal polynomials are listed in Table 2. Note that $\mathcal{P}_{000}$, $\mathcal{P}_{001}$, $\mathcal{P}_{002}, \ldots$ are pure polynomials in ζ, $\mathcal{P}_{010}, \mathcal{P}_{020}, \ldots$ are polynomials in both η and ζ and $\mathcal{P}_{100}, \mathcal{P}_{200}, \ldots$ are polynomials in all three variables. The properties of the Legendre and Jacobi polynomials ensure

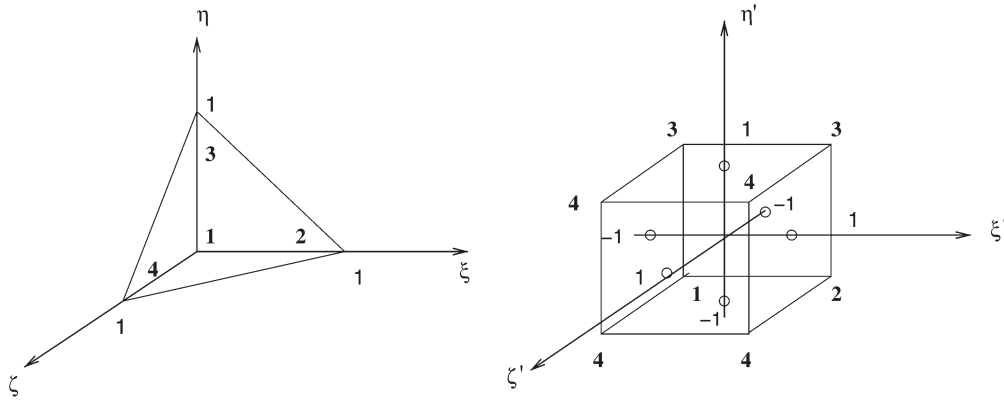

FIG. 2. Mapping of the standard orthogonal tetrahedron in the $\xi\eta\zeta$ space to a cube in the $\xi'\eta'\zeta'$ space.

TABLE 2 *List of the constant, linear and quadratic orthogonal polynomials over the tetrahedron*

$\mathcal{P}_{000} = 1$
$\mathcal{P}_{100} = 2\xi + \eta + \zeta - 1$
$\mathcal{P}_{010} = 3\eta + \zeta - 1$
$\mathcal{P}_{001} = 4\zeta - 1$
$\mathcal{P}_{200} = 6\xi^2 + \eta^2 + \zeta^2 + 6\xi\eta + 6\xi\zeta + 2\eta\zeta - 6\xi - 2\eta - 2\zeta + 1$
$\mathcal{P}_{110} = 5\eta^2 + \zeta^2 + 10\xi\eta + 2\xi\zeta + 6\eta\zeta - 2\xi - 6\eta - 2\zeta + 1$
$\mathcal{P}_{101} = 6\zeta^2 + 12\xi\zeta + 6\eta\zeta - 2\xi - \eta - 7\zeta + 1$
$\mathcal{P}_{020} = 10\eta^2 + \zeta^2 + 8\eta\zeta - 8\eta - 2\zeta + 1$
$\mathcal{P}_{011} = 6\zeta^2 + 18\eta\zeta - 3\eta - 7\zeta + 1$
$\mathcal{P}_{002} = 15\zeta^2 - 10\zeta + 1$

that (2.2) satisfies the orthogonality relation

$$\iiint_T \mathcal{P}_{klp}\mathcal{P}_{qrs}\,\mathrm{d}\xi\,\mathrm{d}\eta\,\mathrm{d}\zeta = 0, \tag{2.3}$$

when $k \neq q$, $l \neq r$ or $p \neq s$, where the integration is performed over the volume of the standard tetrahedron, T. The self-projection is given by

$$\mathcal{G}_{klp} = \iiint_T \mathcal{P}_{klp}^2\,\mathrm{d}\xi\,\mathrm{d}\eta\,\mathrm{d}\zeta = \frac{1}{(2k+1)(2k+2l+2)(2k+2l+2p+3)}. \tag{2.4}$$

Comparing this formula with a corresponding result for the Proriol (1957) orthogonal polynomials defined over the triangle (Blyth & Pozrikidis, 2005) suggests a simple formula for the simplex.

The tetrahedral orthogonal polynomials provide us with a complete orthogonal base. Any function, $f(\xi, \eta, \zeta)$, defined over the standard tetrahedron in the $\xi\eta\zeta$ space, can be approximated with a complete mth-degree polynomial in ξ, η and ζ, expressed in the form

$$f(\xi, \eta, \zeta) = \sum_{k=0}^{m}\sum_{l=0}^{m-k}\sum_{p=0}^{m-k-l} a_{klp}\mathcal{P}_{klp}(\xi, \eta, \zeta), \tag{2.5}$$

where the triple sum is designed so that $k + l + p \leqslant m$. Multiplying (2.5) by $\mathcal{P}_{klp}$, integrating over the volume of the standard tetrahedron and using the orthogonality property, we find that the expansion coefficients are given by

$$a_{klp} = \frac{1}{\mathcal{G}_{klp}} \iiint_T f(\xi, \eta, \zeta)\mathcal{P}_{klp}(\xi, \eta, \zeta)\mathrm{d}\xi\,\mathrm{d}\eta\,\mathrm{d}\zeta, \tag{2.6}$$

where $\mathcal{G}_{klp}$ is defined in (2.4). The terms in (2.5) can be arranged into a Pascal pyramid consisting of a stack of Pascal triangles with increasing dimensions. The first triangle is a point representing the constant term

$$\mathcal{P}_{000},$$

the second triangle encapsulates the linear functions

$$\begin{matrix} \mathcal{P}_{100} \\ \mathcal{P}_{010} \quad \mathcal{P}_{001}, \end{matrix}$$

the third triangle encapsulates the quadratic functions

$$\begin{matrix} \mathcal{P}_{200} \\ \mathcal{P}_{110} \quad \mathcal{P}_{101} \\ \mathcal{P}_{020} \quad \mathcal{P}_{011} \quad \mathcal{P}_{002} \end{matrix}$$

and the $(m + 1)$th triangle encapsulates the mth-order functions. To convert a monomial product series into the equivalent orthogonal polynomial series, we use the expressions given in Table 3.

TABLE 3 *Expressions of monomials products in terms of the tetrahedral orthogonal polynomials*

$1 = \mathcal{P}_{000}$
$\xi = \frac{1}{12}(3\mathcal{P}_{000} + 6\mathcal{P}_{100} - 2\mathcal{P}_{010} - \mathcal{P}_{001})$
$\eta = \frac{1}{12}(3\mathcal{P}_{000} + 4\mathcal{P}_{010} - \mathcal{P}_{001})$
$\zeta = \frac{1}{4}(\mathcal{P}_{000} + \mathcal{P}_{001})$
$\xi^2 = \frac{1}{90}(9\mathcal{P}_{000} + 30\mathcal{P}_{100} - 10\mathcal{P}_{010} - 5\mathcal{P}_{001} + 15\mathcal{P}_{200} - 9\mathcal{P}_{110} - 6\mathcal{P}_{101} + 3\mathcal{P}_{020} + 2\mathcal{P}_{011} + \mathcal{P}_{002})$
$\eta^2 = \frac{1}{90}(9\mathcal{P}_{000} + 20\mathcal{P}_{010} - 5\mathcal{P}_{001} + 9\mathcal{P}_{020} - 4\mathcal{P}_{011} + \mathcal{P}_{002})$
$\zeta^2 = \frac{1}{30}(3\mathcal{P}_{000} + 5\mathcal{P}_{001} + 2\mathcal{P}_{002})$
$\xi\eta = \frac{1}{180}(9\mathcal{P}_{000} + 15\mathcal{P}_{100} + 5\mathcal{P}_{010} - 5\mathcal{P}_{001} + 18\mathcal{P}_{110} - 3\mathcal{P}_{101} - 9\mathcal{P}_{020} - \mathcal{P}_{011} + \mathcal{P}_{002})$
$\xi\zeta = \frac{1}{180}(9\mathcal{P}_{000} + 15\mathcal{P}_{100} - 5\mathcal{P}_{010} + 5\mathcal{P}_{001} + 15\mathcal{P}_{101} - 5\mathcal{P}_{011} - 4\mathcal{P}_{002})$
$\eta\zeta = \frac{1}{180}(9\mathcal{P}_{000} + 10\mathcal{P}_{010} + 5\mathcal{P}_{001} + 10\mathcal{P}_{011} - 4\mathcal{P}_{002})$

3. Lobatto grid over the tetrahedron

In the proposed distribution, Lobatto triangle interpolation nodes are distributed over the faces of the tetrahedron, as follows:

- On the $\xi\eta$ face, nodes are distributed at

$$\xi = \frac{1}{3}(1 + 2v_i - v_j - v_l), \quad \eta = \frac{1}{3}(1 - v_i + 2v_j - v_l), \quad \zeta = 0, \tag{3.1}$$

  for $i = 1, 2, \ldots, m+1$ and $j = 1, 2, \ldots, m+2-i$, where $l = m + 3 - i - j$.

- On the $\eta\zeta$ face, nodes are distributed at

$$\xi = 0, \quad \eta = \frac{1}{3}(1 + 2v_j - v_k - v_l), \quad \zeta = \frac{1}{3}(1 - v_j + 2v_k - v_l), \tag{3.2}$$

  for $j = 1, 2, \ldots, m$ and $k = 2, 3, \ldots, m+2-j$, where $l = m + 3 - j - k$.

- On the $\zeta\xi$ face, nodes are distributed at

$$\xi = \frac{1}{3}(1 + 2v_i - v_k - v_l), \quad \eta = 0, \quad \zeta = \frac{1}{3}(1 - v_i + 2v_k - v_l), \tag{3.3}$$

  for $i = 2, 3, \ldots, m$ and $k = 2, 3, \ldots, m+2-i$, where $l = m + 3 - i - k$.

- On the slanted face, nodes are distributed at

$$\xi = \frac{1}{3}(1 + 2v_i - v_j - v_l), \quad \eta = \frac{1}{3}(1 - v_i + 2v_j - v_l), \quad \zeta = 1 - \xi - \eta, \tag{3.4}$$

  for $i = 2, 3, \ldots, m$ and $j = 2, 3, \ldots, m+1-i$, where $l = m + 3 - i - j$.

Note that the range of indices has been adjusted so that each node is uniquely defined. The resulting node distributions over the faces of the tetrahedron for $m = 3$ and 4 are shown in Fig. 3.

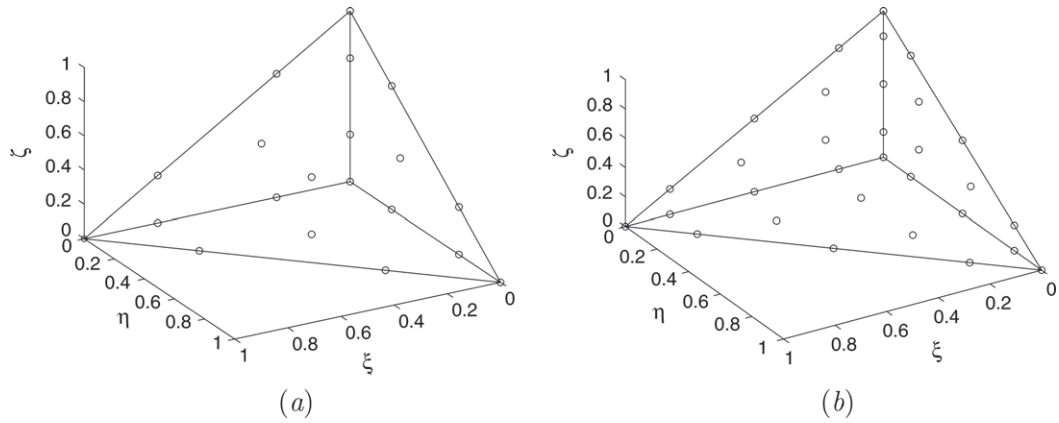

FIG. 3. (a) A 20-node tetrahedron supporting a complete cubic expansion, $m = 3$ and (b) a 35-node tetrahedron supporting a complete quartic expansion, $m = 4$. For clarity, only the face nodes in the three orthogonal planes are show in (b).

3.1 *Lobatto grid with optimized interior nodes*

In the first approach, the interior nodes arising for $m \geqslant 4$ are found by maximizing the magnitude of the determinant of the generalized VDM, $\det(\mathbf{V})$. The matrix itself is written with respect to the orthogonal polynomial base discussed in Section 2. Though the modal expansion base is somewhat preferable in that only the portion of the matrix corresponding to the interior nodes must be considered, as discussed by Chen & Babuška (1996), the orthogonal base makes for a simpler bookkeeping.

The optimization algorithm is a variation of the conjugate-gradients method, known as the Polak–Ribiere algorithm (Press *et al.*, 1986, New york, Cambridge University Press). First, an initial guess is made for the coordinates of the interior nodes encapsulated in the vector $\mathbf{x}$. Subsequently, the update directions, $\mathbf{p}^n$, are computed as

$$\mathbf{p}^1 = \mathbf{g}^1 \quad \text{and} \quad \mathbf{p}^n = \mathbf{g}^n + \beta^n \mathbf{p}^{n-1} \ \text{ for } \ n > 1, \tag{3.5}$$

where $\mathbf{g} = \nabla \det(\mathbf{V})$ is the gradient, and

$$\beta^n = \frac{(\mathbf{g}^n - \mathbf{g}^{n-1}) \cdot \mathbf{g}^n}{\mathbf{g}^{n-1} \cdot \mathbf{g}^{n-1}}. \tag{3.6}$$

The nodal position vector is updated as

$$\mathbf{x}^{n+1} = \mathbf{x}^n + \alpha^n \mathbf{p}^n, \tag{3.7}$$

where the step size, α^n, is found by maximizing the magnitude of $\det(\mathbf{V})$ along the update direction, $\mathbf{p}^n$, using a 1D searching algorithm such as Brent's method (Press *et al.*, 1986, New York, Cambridge University Press), subject to the constraint that the nodes lie inside the tetrahedron. The derivatives defining the gradient $\mathbf{g}$ are computed using the formula

$$g_i^{(k)} = \frac{\partial \det(\mathbf{V})}{\partial x_i^{(k)}} = (-1)^{i+j} \det(\mathbf{A}^{ji}) \frac{\partial \phi_j}{\partial x_i^{(k)}} = \det(\mathbf{V}) \bar{V}_{ij} \frac{\partial \phi_j}{\partial x_i^{(k)}}, \tag{3.8}$$

where $x_i^{(k)}$ is the kth coordinate of the ith node, $\mathbf{A}^{ji}$ is the matrix cofactor of $\mathbf{V}$ associated with the element V_{ji} and $\bar{V}_{ij}$ are the elements of the inverse of the VDM, $\bar{\mathbf{V}} = \mathbf{V}^{-1}$.

The accuracy of the minimizer is limited by the finite precision in the computation of the determinant of $\mathbf{V}$. To sharpen the optimization, at the end of the conjugate-gradient module, the system of non-linear equations, $\mathbf{g} = 0$, is solved using Newton's method using the Hessian matrix

$$H_{ik}^{(pq)} = \frac{\partial g_i^{(p)}}{\partial x_k^{(q)}} = \frac{\partial}{\partial x_k^{(q)}}\left((-1)^{i+j}\det(\mathbf{A}^{ji})\frac{\partial \phi_j}{\partial x_i^{(p)}}\right)$$
$$= \begin{cases} (-1)^{i+j}\det(\mathbf{A}^{ji})\frac{\partial^2 \phi_j}{\partial x_i^{(p)} x_k^{(q)}}, & \text{for } k = i, \\ (-1)^{i+j}\det(\mathbf{A}^{ji})\bar{A}_{kl}^{ji}\frac{\partial \phi_{\tilde{l}}}{\partial x_k^{(q)}}\frac{\partial \phi_j}{\partial x_i^{(p)}}, & \text{for } k < i, \\ (-1)^{i+j}\det(\mathbf{A}^{ji})\bar{A}_{\tilde{k}l}^{ji}\frac{\partial \phi_{\tilde{l}}}{\partial x_k^{(q)}}\frac{\partial \phi_j}{\partial x_i^{(p)}}, & \text{for } k > i, \end{cases} \tag{3.9}$$

where $\bar{A}_{kl}^{ji}$ are elements of the matrix $\bar{\mathbf{A}}^{ji} = (\mathbf{A}^{ji})^{-1}$, $\tilde{k} = k-1$, $\tilde{l} = l$ for $l < j$ and $\tilde{l} = l+1$ for $l \geqslant j$.

Because the optimization is sensitive to the initial guess and easily swayed by a local minimum, a good initial guess is required. For a symmetric nodal distribution corresponding to polynomial degree, m, the interior nodal structure resembles the full structure of the $(m-4)$th-degree polynomial expansion shrunk by a certain factor with respect to the tetrahedron centroid. In our computations, an improved $(m-4)$th-degree nodal set is initially constructed by uniformly shrinking the corresponding set by an optimal ratio towards the centre of the tetrahedron. The optimal ratio was obtained by solving a 1D optimization problem using Brent's method with the goal of maximizing $|\det(\mathbf{V})|$. The optimized shrinking ratios for $m = 5, 6, 7, 8$ and 9, are found to be, respectively, 0.28001, 0.46863, 0.58557, 0.66704 and 0.72627.

3.2 *Lobatto grid over the tetrahedron*

In the second approach, interior nodes are heuristically introduced based on the master grid defined in (1.11), at positions

$$\xi = \frac{1}{4}(1 + 3v_i - v_j - v_k - v_l),$$
$$\eta = \frac{1}{4}(1 - v_i + 3v_j - v_k - v_l), \tag{3.10}$$
$$\zeta = \frac{1}{4}(1 - v_i - v_j + 3v_k - v_l),$$

for $i = 2, 3, \ldots, m$, $j = 2, 3, \ldots, m+1-i$ and $k = 2, 3, \ldots, m+2-i-j$, where $l = m+4-i-j-k$. Note that the range of subscripts restricts the nodes inside the tetrahedron. Since both the interior and boundary nodes are based on the 1D completed Lobatto points, we refer to this set as the Lobatto tetrahedral (LTT) set. Formula (3.10) together with (3.1)–(3.4) ensures that the LTT distribution observes five groups of multi-fold symmetries with respect to the $\xi\eta\zeta$ coordinates, as discussed in Chen & Babuška (1996). The symmetry of the LTT is evident in Fig. 4 where the full nodal sets for $m = 5$ and 6 are displayed. Figure 5 compares the interior node distributions obtained by the two methods discussed in this section for $m = 5$ and 6, and demonstrates that the differences are small.

If the range of subscripts in Formula (3.10) is extended such that $i = 1, 2, \ldots, m+1$, $j = 1, 2, \ldots, m+2-i$ and $k = 1, 2, \ldots, m+3-i-j$, a complete set of N nodes will arise. However,

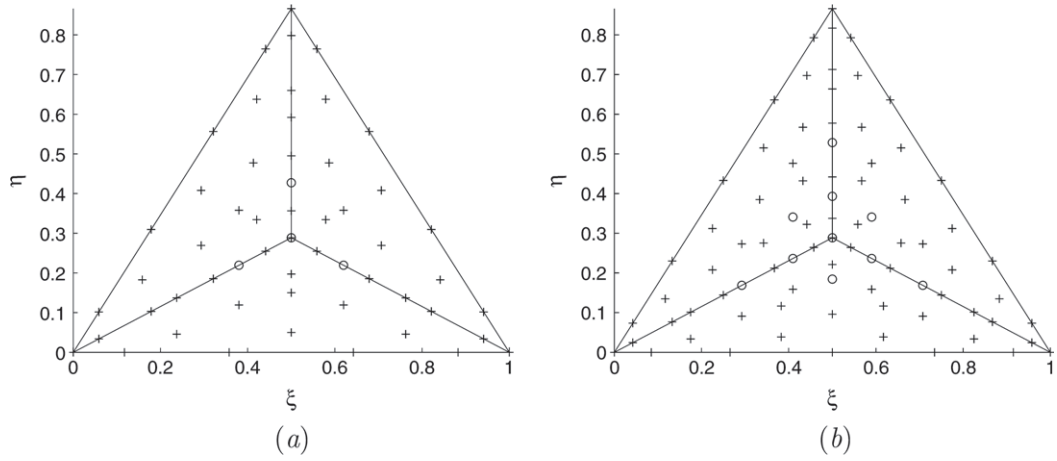

FIG. 4. Multi-fold symmetry of the LTT distribution over the regular tetrahedron (top view) for (a) $m = 5$ and (b) $m = 6$. The interior points are shown as circles and the boundary points are shown as crosses.

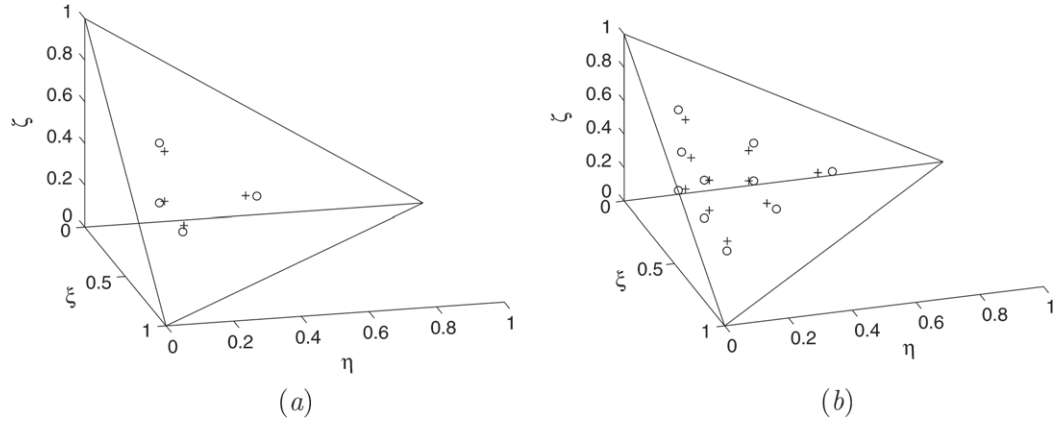

FIG. 5. Comparison of the interior nodal distributions for (a) $m = 5$ and (b) $m = 6$, over an orthogonal tetrahedron obtained by optimization (o) and Formula (3.10) (+).

the peripheral nodes produced by the extended formula do not always lie in the faces of the tetrahedron. An example of an anomalous distribution is shown in Fig. 6 for $m = 4$, where only the peripheral nodes located near the three orthogonal faces are displayed. The extended formula produces some peripheral nodes that correspond to the completed Lobatto points along each edge, but does not necessarily produce nodes that lie within the triangular faces, as required. It is for this reason that Formula (3.10) is combined with the LTR distribution to generate a complete set.

4. Properties of the Lobatto tetrahedral sets

To assess the properties of the two grids proposed in Section 3, we consider the Lebesgue constant,

$$\Lambda_N \equiv \max_{\mathbf{x}\in T}\{\mathcal{L}_N(\mathbf{x})\}, \tag{4.1}$$

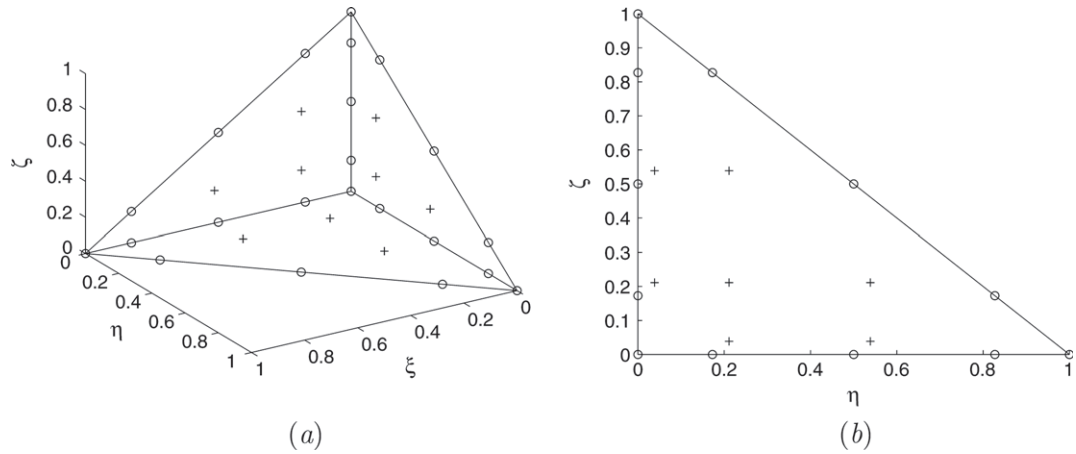

FIG. 6. Peripheral nodes near the three orthogonal faces of the tetrahedron produced by extending the range of the subscripts in Formula (3.10) for $m = 4$. The nodes include the Lobatto points along the edges (o); the rest of the nodes (+) do not lie in the faces of the tetrahedron, but are slightly displaced towards the interior of the domain; (a) oblique and (b) side view.

where the point $\mathbf{x} = (\xi, \eta, \zeta)$ lies in the tetrahedron, T, and $\mathcal{L}_N$ is the Lebesgue function,

$$\mathcal{L}_N(\mathbf{x}) = \sum_{i=1}^{N} |\psi_i(\mathbf{x})|. \tag{4.2}$$

To compute the ith cardinal interpolation function, $\psi_i(\xi, \eta, \zeta)$, we may expand it into a series of orthogonal tetrahedral polynomials using (2.5),

$$\psi_i(\xi, \eta, \zeta) = \sum_{j=0}^{m} \sum_{k=0}^{m-j} \sum_{l=0}^{m-j-k} a_{jkl}^{(i)} \mathcal{P}_{jkl}(\xi, \eta, \zeta) \equiv \sum_{j=1}^{N} b_j^{(i)} \phi_j(\xi, \eta, \zeta), \tag{4.3}$$

and then compute the coefficients $b_j^{(i)}$ by solving the Vandermonde system

$$\mathbf{V}^{\mathrm{T}} \cdot \mathbf{b}^{(i)} = \mathbf{e}^{(i)}, \tag{4.4}$$

where $V_{jk} \equiv \phi_j(\xi_k, \eta_k, \zeta_k)$, and $\mathbf{e}_i$ is the N-dimensional unit vector in the ith direction. Thus,

$$\psi_i(\xi, \eta, \zeta) = \mathbf{e}^{(i)} \cdot \mathbf{V}^{-1} \cdot \boldsymbol{\phi}, \tag{4.5}$$

or

$$\psi_i(\xi, \eta, \zeta) = \sum_{k=1}^{N} V_{ik}^{-1} \phi_k(\xi, \eta, \zeta). \tag{4.6}$$

This formula also arises directly by using the Lagrange interpolation formula to write

$$\phi_j(\xi, \eta, \zeta) = \sum_{k=1}^{N} V_{jk} \psi_k(\xi, \eta, \zeta). \tag{4.7}$$

TABLE 4 *Condition number, $\sigma(\mathbf{V})$, of the VDM defined using the orthogonal tetrahedral polynomials as basis functions*

m	3	4	5	6	7	8	9
Optimized interior	15.7	34.3	65.4	129.3	235.0	418.9	779.9
LTT	15.7	34.3	64.8	120.7	198.9	333.6	568.5

TABLE 5 *Comparison of the Lebesgue constant, Λ_N, for different distributions over the tetrahedron*

m	LTT	Optimized interior	Chen and Babuška (L_2 set)	Chen and Babuška (VDM set)	Hesthaven and Teng
2	2.0	2.0	2.0	2.0	2.0
3	2.93	2.93	2.93	2.93	2.93
4	4.07	4.07	4.11	4.15	4.08
5	5.38	5.70	5.62	6.00	5.35
6	7.53	8.84	7.36	8.89	7.34
7	10.17	11.48	9.37	11.64	9.76
8	14.63	15.52	12.31	15.83	13.63
9	20.46	19.76	15.69	22.33	18.90

Typical values of the condition number of the VDM, $\sigma(\mathbf{V}) = \|\mathbf{V}\|\|\mathbf{V}^{-1}\|$, computed using Matlab, are shown in Table 4. It is interesting to observe that, for high polynomial orders, m, the LTT gives a condition number that is lower than that of the distribution with optimized interior points.

To compute the Lebesgue constant, we introduce a uniform Cartesian grid, calculate the Lebesgue function at the grid nodes by exploiting geometrical symmetries and perform a direct search for the maximum. The rough maximum is subsequently refined by performing a gradient-based local maximization. Table 5 shows the Lebesgue constants for the optimized interior and LTT distributions, together with the corresponding values for the Chen & Babuška (1996) and Hesthaven & Teng (2000) distributions. For m up to 3, all distributions are identical. For $m > 3$, the Lebesgue constants for the Lobatto grid are lower than those for the VDM grid obtained by Chen and Babuška, while comparing favourably with those of the L_2 set obtained by Chen and Babuška and the electrostatics set obtained by Hesthaven and Teng.

As a practical test of the interpolation accuracy, we consider several test functions and compute the infinity norm of the interpolation error defined as

$$L_\infty(f) = \|p_m - f\|_\infty = \max_{\mathbf{x}\in T} |p_m(\mathbf{x}) - f(\mathbf{x})|. \tag{4.8}$$

The infinity norm is evaluated directly by computing the maximum error over the volume of the standard tetrahedron discretized into a large number of intervals. Table 6 shows the infinity norm of the error for three selected functions and various degrees of interpolation. Both the LTT and the optimized interior grid presented in Section 3 outperform the uniform grid.

Of particular interest is the 3D Runge function defined as

$$f_R(\xi, \eta, \zeta) = \frac{1}{1 + 100(\xi - 0.5)^2} \frac{1}{1 + 100(\eta - 0.5)^2} \frac{1}{1 + 100(\zeta - 0.5)^2}, \tag{4.9}$$

TABLE 6 *Interpolation error measured by the infinity norm, $L_\infty(f)$, over the tetrahedron, for three test functions, $f_1 = \cos(5\xi)\sin(5\eta)\cos(5\zeta)$, $f_2 = \cos(10\xi)e^{2\eta}\cos(10\zeta)$ and f_R is the 3D Runge function defined in the text*

Function	m	1	3	6	9	12
f_1	Uniform grid	1.3197	0.8896	0.1909	0.0062	3.1613×10^{-4}
	LTT	1.3197	0.6756	0.1334	0.0014	1.1617×10^{-4}
	Optimized interior	1.3197	0.6756	0.1334	0.0013	—
f_2	Uniform grid	9.0610	4.1821	2.6333	1.7350	0.4884
	LTT	9.0610	3.9720	1.6512	0.4493	0.0877
	Optimized interior	9.0610	3.9720	1.6512	0.4493	—
f_R	Uniform grid	0.0412	0.0356	0.0467	0.0572	0.4278
	LTT	0.0412	0.0370	0.0190	0.0203	0.0168
	Optimized interior	0.0412	0.0370	0.0190	0.0203	—

plotted in Fig. 7(a) in the plane $\xi = 0$. Note that the coefficients in this expression have been adjusted to account for the unit length of the tetrahedral edges, and the axes have been shifted to the midpoint of the three orthogonal edges. The interpolation accuracy of the 1D Runge function over the interval $[-1, 1]$ is known to rapidly worsen as the polynomial order is raised on the uniform grid (e.g. Pozrikidis, 1998, p. 278, 2005). In three dimensions, we find a similar poor performance on the uniform grid, with the infinity norm of the error increasing almost linearly with m. The Runge effect is evident in the graphs presented in Fig. 7(b, c), where the interpolating polynomials of degrees $m = 6$ and 12 are plotted in the plane $\xi = 0$. The 12th-degree interpolating polynomial based on the LTT distribution displayed in Fig. 7(d) is a much better approximation.

Finite-element formulations of initial-value problems culminate in first-order ordinary differential equations, where the time derivative of the nodal solution vector is multiplied by the element mass matrix

$$M_{ij} = \iiint_T \psi_i \psi_j \, \mathrm{d}\xi \, \mathrm{d}\eta \, \mathrm{d}\zeta. \tag{4.10}$$

To prevent numerical instability, it is desirable to have a well-conditioned mass matrix. Using (4.6) and the orthogonality property, we find that the mass matrix can be expressed as

$$M_{ij} = V_{ik}^{-1} V_{jl}^{-1} \iiint_T \phi_k \phi_l \, \mathrm{d}\xi \, \mathrm{d}\eta \, \mathrm{d}\zeta = \sum_{k=1}^{N} V_{ik}^{-1} V_{jk}^{-1} \|\phi_k\|^2, \tag{4.11}$$

where

$$\|\phi_k\|^2 = \iiint_T \phi_k^2 \, \mathrm{d}\xi \, \mathrm{d}\eta \, \mathrm{d}\zeta, \tag{4.12}$$

is evaluated from (2.4). Table 7 shows the condition number of the mass matrix, $\sigma(\mathbf{M})$, for five grids, including the uniform grid. The results show that the condition number of the LTT is comparable to, though generally somewhat higher than that of the Chen and Babuška L_2 grid and the Hesthaven and Teng electrostatics grid. As m is raised, the condition number grows significantly faster for the uniform grid than for all other grids.

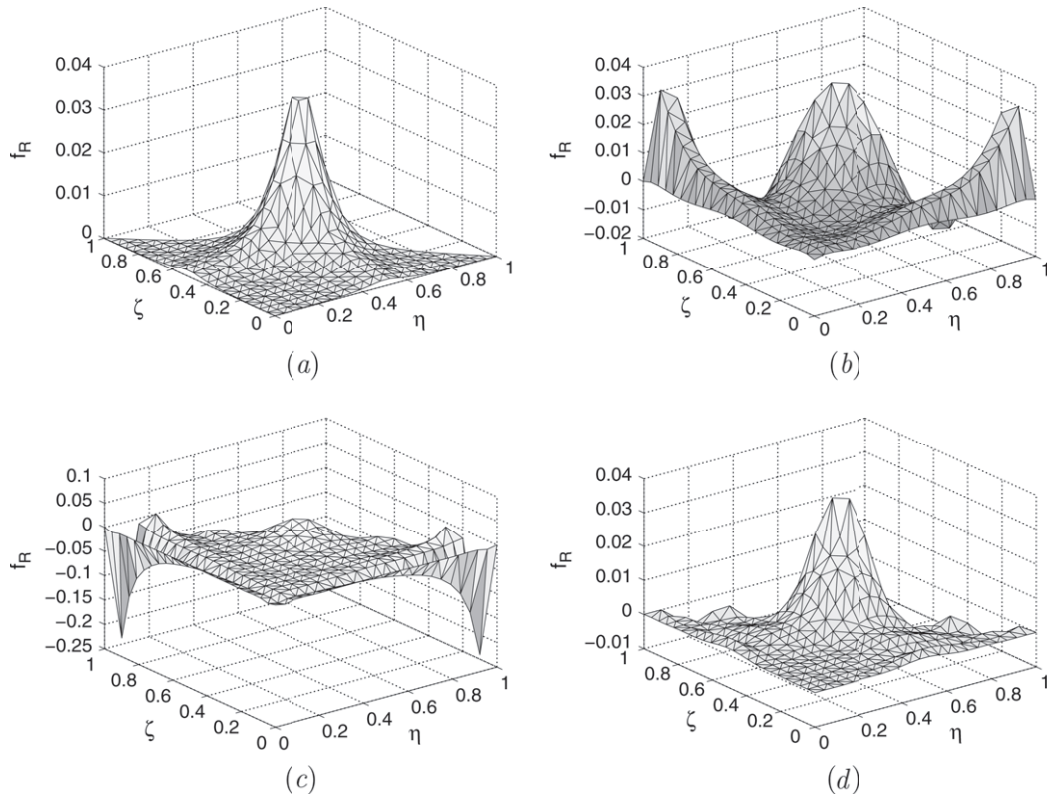

FIG. 7. (a) Graph of the 3D Runge function in the $\xi = 0$ plane. (b, c) The interpolating function for $m = 6$ and 12 on a uniform grid and (d) the interpolating function for $m = 12$ on the LTT.

TABLE 7 *Condition number of the mass matrix, σ (**M**), truncated to its integral part, for five nodal distributions*

m	3	4	5	6	7	8	9
Optimized interior points	110	250	349	833	1582	3979	10915
LTT	110	250	366	704	1514	4048	9876
Chen and Babuška (L_2)	111	252	356	685	1452	3346	7951
Hesthaven and Teng	110	250	352	705	—	3507	9769
Uniform grid	105	237	410	1089	2735	8454	26314

The elements of the diffusion or Laplacian matrix, **D**, may also be computed using (4.6), as

$$D_{ij} \equiv \iiint_T \nabla\psi_i \cdot \nabla\psi_j \,\mathrm{d}\xi\,\mathrm{d}\eta\,\mathrm{d}\zeta = V_{ik}^{-1} V_{jl}^{-1} \iiint_T \nabla\phi_k \cdot \nabla\phi_l \,\mathrm{d}\xi\,\mathrm{d}\eta\,\mathrm{d}\zeta, \tag{4.13}$$

where $\nabla = (\partial/\partial\xi, \partial/\partial\eta, \partial/\partial\zeta)$ is the gradient operator. The diffusion matrices for $m = 1$ and 2 are displayed in Table 8. A Matlab script that produces the matrices for higher-order expansions of the LTT distribution can be obtained from the authors on request.

TABLE 8 *Interpolation node coordinates over the orthogonal tetrahedron and associated diffusion matrix* **D** *for (a)* $m = 1$ *and (b)* $m = 2$

(a)

i	1	2	3	4
ξ_i	0	0	1	0
η_i	0	1	0	0
ζ_i	0	0	0	1

$$\mathbf{D} = \begin{vmatrix} 1/2 & -1/6 & -1/6 & -1/6 \\ -1/6 & 1/6 & 0 & 0 \\ -1/6 & 0 & 1/6 & 0 \\ -1/6 & 0 & 0 & 1/6 \end{vmatrix}$$

(b)

i	1	2	3	4	5	6	7	8	9	10
ξ_i	0	0	0	1/2	1/2	1	0	0	1/2	0
η_i	0	1/2	1	0	1/2	0	0	0	0	1/2
ζ_i	0	0	0	0	0	0	1/2	1	1/2	1/2

$$\mathbf{D} = \begin{vmatrix} 3/10 & -1/5 & 1/30 & -1/5 & 1/15 & 1/30 & -1/5 & 1/30 & 1/15 & 1/15 \\ -1/5 & 4/5 & -2/15 & 2/15 & -4/15 & 1/30 & 2/15 & 1/30 & -4/15 & -4/15 \\ 1/30 & -2/15 & 1/10 & 1/30 & -1/30 & 0 & 1/30 & 0 & 0 & -1/30 \\ -1/5 & 2/15 & 1/30 & 4/5 & -4/15 & -2/15 & 2/15 & 1/30 & -4/15 & -4/15 \\ 1/15 & -4/15 & -1/30 & -4/15 & 8/15 & -1/30 & -4/15 & 0 & 2/15 & 2/15 \\ 1/30 & 1/30 & 0 & -2/15 & -1/30 & 1/10 & 1/30 & 0 & -1/30 & 0 \\ -1/5 & 2/15 & 1/30 & 2/15 & -4/15 & 1/30 & 4/5 & -2/15 & -4/15 & -4/15 \\ 1/30 & 1/30 & 0 & 1/30 & 0 & 0 & -2/15 & 1/10 & -1/30 & -1/30 \\ 1/15 & -4/15 & 0 & -4/15 & 2/15 & -1/30 & -4/15 & -1/30 & 8/15 & 2/15 \\ 1/15 & -4/15 & -1/30 & -4/15 & 2/15 & 0 & -4/15 & -1/30 & 2/15 & 8/15 \end{vmatrix}$$

5. Discussion

We have presented a node construction for interpolating a function over a tetrahedron based on the zeros of the Lobatto polynomials. Our primary concern has been to devise a relatively simple scheme that is straightforward to generate and does not compromise the interpolation accuracy. Previous high-accuracy schemes demand a fair amount of effort to construct the node positions (e.g. Chen & Babuška, 1996; Hesthaven & Teng, 2000).

In developing the new distribution, we have worked in two stages. Firstly, we computed a set of optimized interior nodes subject to the Lobatto triangle (LTR) distribution over each face (Blyth & Pozrikidis 2005), by maximizing the magnitude of the determinant of the VDM. Secondly, we devised a simple formula for the interior nodes as an extension of the LTR distribution. The resulting 3D distribution is coined the LTT. Lebesgue constants for the LTT are superior to those of the VDM set computed by Chen & Babuška (1996), and compare favourably with those of the L_2 set computed by Chen & Babuška (1996) and with the electrostatics set computed by Hesthaven & Teng (2000). The accuracy of the LTT was confirmed by computing the infinity norm of the interpolation error for sample functions. As an added benefit, the condition number of the mass matrix for the LTT was shown to be superior to that for the uniform grid and comparable to that of other optimal grids. In summary, the straightforward construction of the LTT makes it an attractive choice in 3D spectral-element implementations such as those arising in elastodynamics and hydrodynamics.

Acknowledgements

The manuscript benefited from insightful comments by the referees. This research was supported by a grant provided by the National Science Foundation.

REFERENCES

BLYTH, M. G. & POZRIKIDIS, C. (2005) A Lobatto interpolation grid over the triangle. *IMA J. Appl. Math.* (to appear).

CHEN, Q. & BABUŠKA, I. (1996) The optimal symmetrical points for polynomial interpolation of real functions in the tetrahedron. *Comput. Methods Appl. Mech. Eng.*, **137**, 89–94.

HESTHAVEN, J. S. & TENG, C. H. (2000) Stable spectral methods on tetrahedral elements. *SIAM J. Sci. Comput.*, **21**, 2352–2380.

KARNIADAKIS, G. E. & SHERWIN, S. J. (2004) *Spectral/hp Element Methods for CFD*, 2nd edn. New York: Oxford University Press.

POZRIKIDIS, C. (1998) *Numerical Computation in Science and Engineering*. New York: Oxford University Press.

POZRIKIDIS, C. (2005) *Introduction to Finite and Spectral Element Methods Using Matlab*. Boca Raton: Chapman & Hall/CRC.

PRESS, W. H., FLANNERY, B. P., TEUKOLSKY, S. A. & VETTERLING, W. T. (1986) *Numerical Recipes*. New York: Cambridge University Press.

PRORIOL, J. (1957) Sur une famille de polynomes à deux variables orthogonaux dans un triangle. *C. R. Acad. Sci. Paris*, **245**, 2459–2461.

SHERWIN, S. J. & KARNIADAKIS, G. E. (1995) A new triangular and tetrahedral basis for high-order (*hp*) finite element methods. *Int. J. Numer. Methods Eng.*, **38**, 3775–3802.

SHERWIN, S. J. & KARNIADAKIS, G. E. (1996) Tetrahedral *hp* finite elements: algorithms and flow simulations. *J. Comp. Phys.*, **124**, 14–45.

TAYLOR, M. A., WINGATE, B. A. & VINCENT, R. E. (2000) An algorithm for computing Fekete points in the triangle. *SIAM J. Numer. Anal.*, **38**, 1707–1720.